Absence of TXNIP in Humans Leads to Lactic Acidosis and Low Serum Methionine Linked to Deficient Respiration on Pyruvate

Yurika Katsu-Jiménez,[1] Carmela Vázquez-Calvo,[1] Camilla Maffezzini,[2] Maria Halldin,[3] Xiaoxiao Peng,[1] Christoph Freyer,[2] Anna Wredenberg,[2] Alfredo Giménez-Cassina,[1,4] Anna Wedell,[5,6] and Elias S.J. Arnér[1]

Diabetes 2019;68:709–723 | https://doi.org/10.2337/db18-0557

Thioredoxin-interacting protein (TXNIP) is an α-arrestin that can bind to and inhibit the antioxidant protein thioredoxin (TXN). TXNIP expression is induced by glucose and promotes β-cell apoptosis in the pancreas, and deletion of its gene in mouse models protects against diabetes. TXNIP is currently studied as a potential new target for antidiabetic drug therapy. In this study, we describe a family with a mutation in the *TXNIP* gene leading to nondetectable expression of TXNIP protein. Symptoms of affected family members include lactic acidosis and low serum methionine levels. Using patient-derived TXNIP-deficient fibroblasts and myoblasts, we show that oxidative phosphorylation is impaired in these cells when given glucose and pyruvate but normalized with malate. Isolated mitochondria from these cells appear to have normal respiratory function. The cells also display a transcriptional pattern suggestive of a high basal activation of the Nrf2 transcription factor. We conclude that a complete lack of TXNIP in human is nonlethal and leads to specific metabolic distortions that are, at least in part, linked to a deficient respiration on pyruvate. The results give important insights into the impact of TXNIP in humans and thus help to further advance the development of antidiabetic drugs targeting this protein.

Thioredoxin (TXN)–interacting protein (TXNIP), also known as TXN-binding protein 2 (TBP-2) or vitamin D3–upregulated protein 1 (VDUP1), was originally identified as a vitamin D3 target gene in a cancer cell line (1). It was later found to bind and inhibit TXN, thus controlling TXN activity and cellular redox homeostasis (2,3). The TXN system is a major cellular system for control of redox state, antioxidant defense, and several signaling pathways (3,4). The relevance of the TXN system is underscored by the fact that its aberrations are related to onset and/or progression of several pathologies (3,5). In this regard, due to its direct interactions with TXN, the role of TXNIP in control of cellular redox balance has been largely studied (3,6). However, it also seems clear that TXNIP has several additional functions not necessarily related to its inhibition of TXN, including activation of the NLRP3 inflammasome (3,7–9) and suppression of the activities of the nuclear factor (erythroid-derived 2)–like 2 (Nrf2) transcription factor (10). This is interesting, because Nrf2 also suppresses TXNIP expression (11), which yields a complex web of possible regulation pathways among TXNIP, TXN, Nrf2, and the inflammasome since TXN and Nrf2 are also intimately linked with each other as well as with NLRP3 inflammasome activation (10,12,13). It is also

[1]Division of Biochemistry, Department of Medical Biochemistry and Biophysics, Karolinska Institutet, Stockholm, Sweden
[2]Division of Molecular Metabolism, Department of Medical Biochemistry and Biophysics, Karolinska Institutet, Stockholm, Sweden
[3]Department of Women's and Children's Health, Akademiska University Hospital, Uppsala, Sweden
[4]Department of Molecular Biology, Centro de Biología Molecular "Severo Ochoa," Universidad Autónoma de Madrid, Madrid, Spain
[5]Department of Molecular Medicine and Surgery, Science for Life Laboratory, Karolinska Institutet, Stockholm, Sweden
[6]Centre for Inherited Metabolic Diseases, Karolinska University Hospital, Stockholm, Sweden

Corresponding author: Elias S.J. Arnér, elias.arner@ki.se

Received 23 May 2018 and accepted 21 January 2019

This article contains Supplementary Data online at http://diabetes.diabetesjournals.org/lookup/suppl/doi:10.2337/db18-0557/-/DC1.

Y.K.-J. and C.V.-C. are co-first authors.

A.G.-C., A.W., and E.S.J.A. are co-senior authors.

C.V.-C. is currently affiliated with the Department of Molecular Biosciences, Wenner-Gren Institute, Stockholm University, Stockholm, Sweden.

X.P. is currently affiliated with the Strategic Investment Department, Coastal International Holdings Limited, Shenzhen, China.

noteworthy that Nrf2 activation has major metabolic effects, it channels glucose to anabolic and reductive pathways, and its activation seems to protect from development of diabetes (14,15). These observations collectively suggest that although TXNIP activities may affect cellular redox control by binding and inhibiting TXN, its activities may also be related to signaling events that are not necessarily linked to its direct inhibition of TXN and should be considered in relation to Nrf2 activation.

TXNIP is an ~43-kDa protein that belongs to the α-arrestin family of proteins. The α-arrestins are known as multifunctional scaffolding proteins involved in protein–protein interactions that mediate a wide array of signaling processes (16). Indeed, compelling evidence has shown a role for TXNIP in metabolic control partially independent of its ability to bind TXN. A series of genetic analyses to pinpoint mutations involved in a spontaneous mouse model of familial hyperlipidemia led to the identification of a nonsense mutation in the *Txnip* gene (17,18). Subsequent studies using *Txnip*-null mouse genetic models have revealed an important role of TXNIP in regulation of metabolism. *Txnip*-knockout mice fail to coordinate the transition between the fed and fasted states, as they fail to maintain normoglycemia upon fasting, and they display abnormally high ketosis and plasma levels of fatty acids compared with their control counterparts (19,20). TXNIP correspondingly appears to be an important regulator of glucose homeostasis by fine-tuning gluconeogenesis in the liver (20), and TXNIP contributes to regulation of cardiac energy metabolism (21,22). *Txnip* deficiency in mice fed a high-fat diet promotes enhanced adipogenesis while preserving insulin sensitivity (23), and even in the strong diabetic mouse model of leptin-deficient BTBR*ob/ob* mice, *Txnip* deficiency protects the pancreatic β-cells from apoptosis and thus the mice from developing diabetes (24).

Importantly, insulin and cellular glucose influx reciprocally regulate *TXNIP* expression in humans, with glucose influx upregulating *TXNIP* expression and insulin suppressing it (25), which is consistent with a recent study revealing that IGF-1 can suppress *TXNIP* expression (26). Although it was shown that *TXNIP* expression was upregulated in patients with type 2 diabetes mellitus, genetic linkage association studies could not identify any variations in the *TXNIP* gene associated with type 2 diabetes mellitus onset or progression (25). Other genome-wide studies have, however, discovered associations between *TXNIP* gene variants and diabetes (27–29). Thus, collectively, several studies have shown that TXNIP promotes diabetes, with hyperglycemia and pancreatic β-cell death, and TXNIP has thereby been proposed as a promising drug target for the treatment of diabetes (8,30). Loss-of-function of TXNIP in humans has, however, not yet been described, and it has remained unknown whether TXNIP is essential in humans or what pathologies its lack of expression may yield.

In this study, we identified a family with three siblings who bear a homozygous point mutation creating a premature stop codon in the *TXNIP* gene, leading to complete absence of detectable TXNIP protein. Our study demonstrates that abolished TXNIP function is nonlethal in humans and leads to a relatively mild metabolic phenotype linked to less efficient utilization of glucose. These results may collectively further support the notion that TXNIP can be a promising antidiabetic drug target in humans.

RESEARCH DESIGN AND METHODS

Ethical Considerations

This study was approved by the regional ethics committee in Stockholm, Sweden. Informed consent was obtained from both parents of the patients.

Genetic Investigations

Whole-exome sequencing was performed on genomic DNA from the subjects using the HiSeq 2500 platform (Illumina) and the Agilent SureSelect Human All Exon V4 whole-exome kit (Agilent, Santa Clara, CA). The resulting sequences were analyzed using our in-house Mutation Identification Pipeline as previously described (31). All called variants are scored and ranked using the Mutation Identification Pipeline–weighted sum model, which uses multiple parameters but emphasizes Mendelian inheritance patterns and conserved, rare, and protein-damaging variants.

Cell Culture

A skin biopsy (on each of the three patients and on voluntary healthy control subjects) and a percutaneous anterior tibial muscle biopsy (on the two patients born 2009 and 2014 and on voluntary healthy control subjects) were performed, with fibroblasts and myoblasts harvested.

Primary skin fibroblasts (passages 7–14) were cultured in minimal essential medium supplemented with GlutaMax I (Thermo Fisher Scientific, Waltham, MA), 10% FBS (Sigma-Aldrich, St. Louis, MO), and penicillin/streptomycin (BioWhittaker, Lonza, Morristown, NJ). Experiments were performed with cells cultured to 70–80% confluence. Culture medium was replaced every 2 to 3 days, and cells were passaged using 0.05% trypsin (Thermo Fisher Scientific).

Primary myoblasts (passages 5–15) were cultured in F-10 mixture supplemented with GlutaMax I (Thermo Fisher Scientific), 10% FBS (Sigma-Aldrich), 2.5 ng/mL basic fibroblast growth factor (Thermo Fisher Scientific), and penicillin/streptomycin. Experiments were performed with cells cultured to 70–80% confluence. Culture medium was replaced every 2 to 3 days (with basic fibroblast growth factor added freshly each time), and cells were passaged using 0.25% trypsin (Thermo Fisher Scientific).

Reconstitution of TXNIP Expression

Human TXNIP was cloned from blood cDNA into the retroviral expression vector pBABE-gateway using Gateway Technology (Thermo Fisher Scientific). In brief, primers

(TXNIP_attB1_3 forward: 5′-**AAAAAGCAGGCTTC**AUGGUGAUGUUCAAGAAGAUC-3′ and TXNIP_attB2_3 reverse: 5′-**AGAAAGCTGGGTC**UCUUCCACAUGCUCACUGC-3′), specific to TXNIP isoform 1 (NM_006472.5), carrying attB adaptor tags (in boldface) were used to clone hTXNIP into pDONR201, followed by recombination into pBABE-gateway following the manufacturer's instructions. The final vector (pBABE-TXNIP) was confirmed by Sanger sequencing.

Patient and control subject fibroblasts were transformed with either empty pBABE-gateway or pBABE-TXNIP using the retroviral phoenix system. For the production of retrovirus, Phoenix-AMPHO cells (ATCC) were transfected using Lipofectamine 3000 reagent (Thermo Fisher Scientific) following the manufacturer's instructions. After 7 h, fresh medium (DMEM-Glutamax [Thermo Fisher Scientific] supplemented with 10% heat-inactivated FBS [Thermo Fisher Scientific]) was added. Medium was harvested and filtered 24, 36, and 48 h after transfection. Retrovirus-containing medium was concentrated using a Retro-X Concentrator (Clontech) following the manufacturer's instructions. Patient or control subject fibroblasts were transduced after addition of 4 μg/mL polybrene (Sigma-Aldrich) and cultured under puromycin selection (0.15 μg/mL).

Mitochondrial Investigations in Isolated Muscle Mitochondria and Specific Substrate Respiration in Permeabilized Cells

Muscle mitochondria were isolated, and ATP production rate as well as respiratory chain enzyme activities were determined as described (32). To determine mitochondrial respiration in myoblasts of specific complexes using selective mitochondrial substrates, an oxygraph chamber (OROBOROS) was used at 37°C. Basal respiration was measured in MIR05 medium, followed by permeabilization with 4.07 μmol/L digitonin. State 3 respiration via complex I was measured with the injection of 5 mmol/L pyruvate and 2.5 mmol/L ADP (pyruvate), followed by the injection of 0.5 mmol/L malate (malate). Complex II activity (succinate) was determined by the addition of 0.5 μmol/L rotenone and 10 mmol/L succinate. Maximal respiration (carbonyl cyanide *m*-chlorophenyl hydrazone [CCCP]) was measured after addition of 2 μg/mL oligomycin and titration with 0.5 μmol/L steps of CCCP. Mitochondrial quality was controlled for by cytochrome c addition. Finally, complex III was inhibited with 2.5 μmol/L antimycin A.

Cellular Growth Rate

Growth rate was determined as previously described and based on an increase in protein content as cells grow (33). In brief, human primary myoblasts were seeded on multiwell 6-well plates at a density of 1×10^4 cells/well. Cells were fixed with 4% paraformaldehyde at 0, 1, 3, 5, and 7 days after seeding. Culture medium was changed every 2 days. After fixation, cells were rinsed once with PBS and stained with staining solution (0.2% Coomassie Brilliant Blue R-250, 10% acetic acid, and 40% methanol) for 1 h at room temperature. The staining solution was discarded, and the wells were rinsed eight times with distilled H_2O. Subsequently, 0.5 mL of elution solution (0.1 N NaOH in 50% methanol) was added and incubated for 1 h. Finally, 0.5 mL of 10% trichloroacetic acid was added to the well, and 200 μL from each well was transferred to a multi–96-well plate, and absorbance was determined at 595 nm. Growth rate was determined in arbitrary units as an increase in absorbance, setting the starting point at day 0.

TXN and TXN Reductase Levels

The cellular enzymatic activities of TXN and TXN reductase 1 (TXNRD1) were determined using an end-point TXN-dependent insulin reduction assay as previously described (34). The same lysates as those in which activities were measured were also used for the determination of the respective protein levels using Western blots.

RNA Extraction, Reverse Transcription, and Quantitative PCR

Total RNA was extracted using Direct-zol RNA Kits (Zymo Research, Irvine, CA) following the manufacturer's instructions. The yield and purity of the RNA was determined using a Nanodrop spectrophotometer (NanoDrop Technologies, Wilmington, DE). Total RNA (1 μg in 20 μL) was reverse transcribed into cDNA (50 ng/μL final concentration) using the Maxima First Strand cDNA Synthesis Kit for RT-qPCR (Thermo Fisher Scientific), with a mix of random and oligo(dT) hexamer primers. The quantitative PCR was performed from 10 ng of cDNA with the Luminaris Color HiGreen qPCR Master Mix (Thermo Fisher Scientific) with 600 nmol/L primers and using the PikoReal Real-Time PCR System (Thermo Fisher Scientific) with cycling conditions of: 50°C for 120 s; 95°C for 120 s; 40 cycles of 95°C for 15 s plus 55°C for 60 s; and 60°C for 30 s. Primers (Sigma-Aldrich) were designed to span intron–exon boundaries to avoid genomic DNA amplification (all from Sigma-Aldrich). The expression ratio was calculated using the ΔΔ threshold cycle method. β-Actin expression was used to normalize the data and obtain relative expression values with the comparative threshold cycle method. Specificity of the PCR reaction was validated by melting curve analysis. Samples from two patients and two control subjects were separately pooled, and RNA was extracted from five independent plates per pooled samples, derived from separate cultures. The results are from these five independent cultures each measured in duplicate. Primer sequences are available upon request.

Immunofluorescence

Cultured myoblasts were fixed with 4% paraformaldehyde. Cells were permeabilized, and nonspecific binding sites were blocked with 0.1% Triton X-100 and 1% BSA diluted in PBS. Subsequently, cells were stained using primary antibody diluted in the aforementioned blocking solution

followed by incubation with a secondary antibody conjugated with Alexa Fluor dye 594 for red detection (Thermo Fisher Scientific). Nuclei were stained with Solution 8 DAPI PBS Staining Solution (ChemoMetec, Allerod, Denmark), and coverslips were mounted using Fluoromount G (Southern Biotechnology Associates, Birmingham, AL). Samples were examined using an LSM800 laser scanning confocal microscope (Zeiss, Oberkochen, Germany).

Lactate Release as Measure of Glycolytic Rate

Lactate release to the extracellular milieu was used as an indication of glycolytic flux and performed as previously described (35,36). Cells were seeded on M6-multiwell plates at a density of 1.5×10^5 cells/well. The day after, the cells were changed to 1 mL/well of DMEM (Sigma-Aldrich) containing 5 mmol/L glucose. A total of 50 μL of medium was collected at different time points. At the end of the experiment, cells were lysed (see protocol detailed below for cell lysis), and protein content was determined for normalization. The amount of lactate in the medium was determined using the Lactate Reagent (Beckman Coulter, Brea, CA), according to the guidelines provided by the manufacturer. An additional subset of cells in the same conditions, with the presence of 10 mmol/L 2-deoxyglucose, was used to determine the amount of nonglycolytic-derived lactate and was subtracted from the overall lactate production. The results depicted represent glycolysis-derived lactate production.

Extracellular Flux Analysis to Determine Mitochondrial Respiration

Oxygen consumption rate (OCR) in real time was monitored on intact fibroblasts and myoblasts using a Seahorse Extracellular Flux Analyzer XF24-3 (Agilent) as previously described with some modifications (36). Cells were seeded at a density of 5×10^4 cells/well in a final volume of 100 μL. Before the experiment, the cells were changed to bicarbonate- and FBS-free DMEM medium (Sigma-Aldrich) containing either 5 mmol/L glucose plus 1 mmol/L sodium pyruvate or 5 mmol/L sodium malate. After measuring respiration in basal conditions, the fraction of respiration coupled to ATP production was determined by subtracting respiration after addition of the mitochondrial ATP synthase inhibitor oligomycin (0.5 μmol/L) (EMD Millipore, Billerica, MA) from basal respiration. The difference between respiration in the presence of the uncoupling ionophore carbonyl cyanide 4-trifluoromethoxyphenylhydrazone (FCCP) (0.5 μmol/L) (Sigma-Aldrich) and the mitochondrial complex III inhibitor antimycin A (4 μmol/L) (Sigma-Aldrich) allowed us to determine the maximal respiratory capacity in the presence of the aforementioned substrates (glucose plus pyruvate or malate).

Pyruvate Dehydrogenase Activities

For determination of pyruvate dehydrogenase activities, the patient-derived fibroblasts were sent to the National Health Service Highly Specialised Services for rare mitochondrial disorders in Oxford, U.K. (Dr. Garry Brown; see http://mitochondrialdisease.nhs.uk/nhs-mitochondrial-services/oxford/laboratory-and-diagnostic-services-oxford/ for details).

Cell Lysis and Western Blot Analysis

Cells were washed once with PBS, placed on ice, and then homogenized in a buffer containing: 20 mmol/L HEPES, pH 7.4, 100 mmol/L sodium chloride, 100 mmol/L sodium fluoride, 1% Triton X-100, 1 mmol/L sodium orthovanadate (Na_3VO_4), 5 mmol/L EDTA, the Complete Protease Inhibitor Cocktail (Roche Diagnostics, Mannheim, Germany), and PhosStop phosphatase inhibitors (Roche Diagnostics). Samples containing the same amount of protein were mixed with electrophoresis buffer containing SDS, boiled for 5 min, and separated by gel electrophoresis on 4–12% precast acrylamide gels (Thermo Fisher Scientific). The proteins were then transferred to nitrocellulose membranes using an iBlot Dry Blotting system (Thermo Fisher Scientific), and the membranes were blocked with 10% nonfat dried milk in PBS plus 0.2% Tween-20 (PBST). The blocked membranes were incubated overnight with primary antibodies diluted in 5% nonfat dried milk-containing PBST at 4°C. The antibodies used were: TXNIP (1:2,000) (catalog number 40-3700; Invitrogen); β-actin (1:2,000) (catalog number A5441; Sigma-Aldrich); TFAM (1:2,000) (catalog number ab131607; Abcam); NDUFA9 (1:1,000) (catalog number 459100; MitoSciences, Life Technologies); SDHA (1:5,000) (catalog number ab14715; Abcam); UQCRC2 (1:10,000) (catalog number PA5-30204; Thermo Fisher Scientific); COX5a (1:1,000) (catalog number ab110262; Abcam); SDHA (1:5,000) (catalog number ab14715; Abcam); ATP synthase-α subunit (1:1,000) (catalog number 459240; Life Technologies); LDHA (1:1,000) (catalog number 2012; Cell Signaling Technologies); TIM23 (1:1,000) (catalog number 611222; BD Biosciences); TXN (1:500) (catalog number sc58439; Santa Cruz Biotechnology, Dallas, TX); TXNRD1 (1:1,000) (catalog number sc18220; Santa Cruz Biotechnology); and GAPDH (1:1,000) (catalog number sc25778; Santa Cruz Biotechnology).

The membranes were then rinsed three times in PBST and incubated with the corresponding peroxidase-conjugated secondary antibody (Santa Cruz Biotechnology) for 1 h at room temperature. The immunoreactive proteins were visualized by using an enhanced chemiluminescence detection system (Amersham GE Healthcare, Buckinghamshire, U.K.), and subsequent densitometric analysis was performed with a ChemiDoc XRS scanner and Quantity One 4.6.7 Software (Bio-Rad, Hercules, CA).

Imaging

Bright-field images were taken using a Zeiss Axiovert 40 CFL microscope (Zeiss) and photographed with a coupled Zeiss Axiovert ICm1 camera using the Axio Vs40 v4.8.2.0 software (Zeiss).

Statistics

Data are presented as mean ± SEM. Statistical evaluation was performed with the Student *t* test when comparing two groups or two-way ANOVA when comparing several groups using GraphPad Prism software (GraphPad Software, San Diego, CA). Asterisks indicate significant differences between the indicated groups of data sets (*$P < 0.05$; **$P < 0.01$; ***$P < 0.005$).

RESULTS

Identification and Characterization of Patients With a *TXNIP* Gene Mutation Leading to Lack of TXNIP Protein

Patient Characteristics

We investigated a family of Libyan descent with three affected children who all presented with congenital lactic acidosis. There is a fourth child in the family who has compensated transposition of the heart, but no congenital lactic acidosis. The parents are first cousins and normally developed adults. The mother is healthy. The father is rather tall and used to be obese but later reduced his weight to normal and is physically very active.

The first child was a boy born in 2005 who had increased plasma lactate up to maximally 9 mmol/L (normal reference values 0.5–2.2 mmol/L) in the neonatal period. He was treated successfully with dichloroacetic acid (DCA), an acetic acid derivative clinically used to correct lactic acidosis that is believed to increase pyruvate oxidation through inhibition of pyruvate dehydrogenase kinase, which will lower lactic acid production. The boy has since required continuous DCA treatment. Neonatally, he had episodes of hypoglycemia down to 1.8 mmol/L on days 2 and 3, and blood glucose has since been normal. He had no stigmata or overt signs of cardiac, liver, or renal pathologies in the neonatal period. Biochemical investigations of isolated muscle mitochondria at 4 months showed suspected deficiency of complex I of the respiratory chain, but a new evaluation at 3 years gave normal results. At that time, he also had a transient general hyperaminoaciduria. At 3 years, slightly increased AST and alanine aminotransferase levels and a profound hepatomegaly were noted with a homogenous structure on ultrasound. A liver biopsy was performed, revealing increased glycogen storage. Evaluation of plasma amino acid levels showed normal values initially, but eventually deficiency of methionine developed, down to 9 μmol/L (normal reference values 11–42 μmol/L). Serum creatinine levels were often lower than normal, whereas other laboratory investigations have been normal, including plasma triglycerides, homocysteine, and cobalamine (Table 1). The boy is slender and short with thin musculature, but he is developing normally, and his liver size has normalized. He is physically very active, swims a lot, and bikes quite far. We have not measured blood glucose during exercise, but there is no history of low glucose when asking. He has, thus far, a normal development and is doing fine in school.

The second child is a girl born in 2009 who also presented with congenital lactic acidosis, requiring continuous DCA treatment. She had no stigmata and normal organ functions. Like her older brother, she also developed deficiency of plasma methionine, down to 9 μmol/L. Serum creatinine levels were also often low. Laboratory investigations were otherwise normal. Respiratory chain function was normal in isolated muscle mitochondria. Light microscopy of the muscle biopsy showed almost complete dominance of type 1 fibers. The girl is rather tall but growing within the normal target height channel. She is physically very active and, like her older brother, enjoys swimming and bicycling. She has no problems with hypoglycemia when asked, and it has not been measured during exercise. The only somatic problem noted is a mild allergy to thyme, and the girl is developing normally.

The third child is a boy born in 2014, who also had congenital lactic acidosis requiring DCA treatment. He showed failure to thrive during his neonatal period with muscular hypotonus and feeding difficulties. He has been a slow developer and is currently under investigation for problems within autism spectrum disorders. During his first years, he had normal plasma methionine levels, but in the most recent investigations, they were in the low normal range, and during the revision of this paper, he developed deficiency requiring increased methionine substitution therapy, coinciding with the timing of methionine deficiency in his siblings. He still shows slight muscular hypotonus and, like his siblings, has low creatinine levels. He is also tall, but growing within normal target height.

All three children are on continuous treatment with DCA and methionine. For a summary of current glucose, ketone bodies, and additional laboratory findings, see Table 1.

Genetic Investigations

Whole-exome sequencing was performed in the two eldest siblings and the parents, revealing two homozygous single nucleotide variants adjacent to each other in the two siblings in the *TXNIP* gene (NM_006472). The variants were c.174G>T, p.Gln58His and c.175G>T, p.Gly59* (correctly denoted c.174_175delinsTT). The resulting protein change is thus an amino acid substitution at position 58 followed by a truncation. Sanger sequencing confirmed that all three patients were homozygous, whereas both parents were heterozygous for the two mutations. Other inborn errors of metabolism affecting methionine metabolism were excluded. The patients had no additional high-scoring mutations identified following an autosomal-recessive inheritance in any other gene with known function in intermediary metabolism. Neither of the two *TXNIP* mutations were present in the Genome Aggregation Database (gnomAD), which currently spans >123,000 exome and 15,000 whole-genome sequences.

Validation of Lack of TXNIP Expression

We isolated primary fibroblasts and myoblasts from tibial muscle biopsies, which were used for all further characterizations in the current study. Using these cells, we first confirmed by Western blot analysis that the nonsense

Table 1—Glucose homeostasis, ketone bodies, and additional laboratory findings for the three patients described in this study

Patient	Glucose	Ketone bodies	Additional findings
Patient 1: boy, 13 years old	Normal fasting tolerance. Numerous blood gases taken every month for several years, and blood glucose has always been normal. A microdialysis investigation of tissue glucose, glycerol, pyruvate, and lactate at the age of 3 years, with determined metabolite levels every 30th min for 24 h, gave tissue glucose variation between 3.5 (during night) and 5.5 (daytime) mmol/L. A 24 h blood glucose profile at 10 years of age was also performed with samples before meals, 90 min after meals, and twice during nighttime, which gave fasting glucose 5.1 and peak glucose at 1700 h of 7.1 mmol/L. Recently, fasting glucose of 4.3 and 4.7 mmol/L was measured with corresponding fasting insulin of 4.8 and 4.3 μU/mL. HbA_{1c} 26–28 mmol/mol (reference: 28–39) corresponding to 4.5–4.7% NGSP, 83–89 mg/dL eAG, and 4.6–4.9 mmol/L eAG.	At the age of 11 years, fasting β-ketones in blood were 0.5 mmol/L (reference: <0.6 mmol/L). No increased excretion of ketones in urine.	Free fatty acids have not been analyzed. However, fasting glycerol normal with 0.2 mmol/L (reference: 0.02–0.37) and triglycerides also normal. Total cholesterol mostly normal, once elevated to 6.2 mmol/L (reference: 2.9–6.0). HDL 0.8 mmol/L (reference: 0.84–1.9) LDL 4.4 mmol/L (reference: 1.1–3.6) LDL/HDL ratio 5.5 (reference: <5.0) Fasting acylcarnitine and fasting carnitine normal. Cobalamin, folic acid, homocysteine, and methylmalonic acid were all normal. Serum creatinine low in many analyses, with the most recent 27 mmol/L (reference: 44–90).
Patient 2: girl, 9 years old	Normal fasting glucose tolerance. Numerous samples taken every month for several years, and blood glucose has always been normal. A 24 h glucose profile at 5 years of age with samples before meals, 90 min after meals, and twice during nighttime showed a normal variation with fasting glucose 4.8 and peak level 5.6 mmol/L after lunch. More recently, fasting glucose 4.9 and 4.4 mmol/L with corresponding fasting insulin 6.1 and 2.6 μU/mL taken on different days. HbA_{1c} 28–30 mmol/mol (reference: 28–39) corresponding to 4.7–4.9% NGSP, 89–92 mg/dL eAG, and 4.9–5.2 mmol/L eAG.	Two years ago, fasting β-ketones 0.6 (reference: <0.6). No increased urinary excretion. Lactate at the same time was 5.4 mmol/L and glucose 4.4 mmol/L.	Fasting glycerol 0.13 mmol/L (reference: 0.02–0.37). Triglycerides normal, 1.42 mmol/L (reference: 0.42–2.7) Total cholesterol 3.8 mmol/L (reference: 2.9–6.0) HDL 0.99 mmol/L (reference: 0.84–1.9) LDL 2.6 mmol/L (reference: 1.1–3.6) LDL/HDL ratio 2.6 (reference: <5.0) Fasting acylcarnitine and fasting carnitine normal. Cobalamin, folic acid, homocysteine, and methylmalonic acid were all normal. Serum creatinine low in many analyses, the most recent 24 mmol/L (reference: 31–70)
Patient 3: boy, 4 years old	Glucose levels in numerous samples over the years have been normal. A continuous glucose monitoring test was performed for 5 days, and glucose variations remained within normal reference values. HbA_{1c} 29 mmol/mol (reference: 28–39) corresponding to 4.8% NGSP, 91 mg/dL eAG, and 5.1 mmol/L eAG.	No increased urinary excretion.	Triglycerides normal, 1.26 mmol/L (reference: 0.42–2.7) Total cholesterol 3.6 mmol/L (reference: 2.9–6.0) HDL 0.79 mmol/L (reference: 0.84–1.9) LDL 2.3 mmol/L (reference: 1.1–3.6) LDL/HDL ratio 2.9 (reference: <5.0) Fasting acylcarnitine and fasting carnitine normal. Cobalamin, folic acid, homocysteine, and methylmalonic acid were all normal. Serum creatinine low as in his siblings, 16 mmol/L (reference: 31–70)

The table summarizes current laboratory findings for the three patients as assessed during continuous treatment with DCA and methionine. Normal reference values are given in parentheses. eAG, estimated average glucose; NGSP, National Glycohemoglobin Standardization Program.

mutation in the *TXNIP* gene indeed leads to absence of detectable TXNIP protein (Fig. 1*A* and Supplementary Fig. 1*B*).

Patient-Derived Cells Lacking TXNIP Have Normal Growth Rates and Normal Morphology

We next set out to assess whether the absence of TXNIP could lead to alterations in cell growth or cell morphology. We determined cell growth rates in two sets of myoblasts isolated from the patients over the course of 7 days in complete culture medium, which were the same as for cells isolated from healthy donors (Fig. 1*B*). Patient cells displayed no overt morphological alterations compared with control subjects (Fig. 1*C* and Supplementary Fig. 1).

Patient-Derived Cells Lacking TXNIP Have Overtly Normal TXN System Activities and Basally Activated Nrf2 Activity

With TXNIP known as an endogenous TXN inhibitor, we assessed TXN and TXNRD activities in lysates of patient cells but could not detect any apparent effect compared with control subjects (Supplementary Fig. 2). Using quantitative RT-PCR for analysis of Nrf2 target gene transcripts, we found that most of the analyzed target genes were strongly upregulated compared with control subjects, thus suggesting a pronounced basal activation of Nrf2 in the patient myoblasts (Fig. 2).

Patient Myoblasts Lacking TXNIP Have a Deficiency in Respiration on Pyruvate but not on Malate

Considering the lactic acidosis in the TXNIP-deficient patients and effects on glucose utilization in *Txnip*-knockout mice (see INTRODUCTION), we next asked whether the patient-derived cells would display any aberrations in respiration on glucose. Strikingly, patient myoblasts displayed significantly lower mitochondrial respiration in the presence of glucose and pyruvate, both at the basal level and upon uncoupling of mitochondrial respiration with the ionophore FCCP (Fig. 3*A* and *B*). The same was also observed in patient fibroblasts (Supplementary Fig. 3).

Given that *TXNIP*-null myoblasts do not display any obvious morphological or proliferation-related alteration, we hypothesized that they might have adapted their metabolism to compensate for the impaired mitochondrial respiration on glucose and pyruvate. Assessing glycolytic rates by measuring lactate release to the extracellular milieu, this was found to be significantly higher in myoblasts lacking TXNIP than in their control counterparts (Fig. 3*C*). Moreover, when challenged with the mitochondrial ATP-synthase inhibitor oligomycin, glycolytic rates were significantly upregulated in control myoblasts, indicating a shift in metabolic profile toward glycolysis to compensate for the absence of oxidative phosphorylation-derived ATP. However, glycolytic rates in TXNIP-null myoblasts did not change in the presence of oligomycin, suggesting that they were already at a maximal rate of glycolysis (Fig. 3*D*).

To rule out that the significant impairment in glucose-driven oxidative phosphorylation in the TXNIP-null myoblasts was due to a deficiency in the total amount of mitochondria, we determined mitochondrial mass and structure. Performing immunofluorescence and confocal imaging with an antibody against the mitochondrial inner membrane translocase subunit TIM23, we could not see any apparent alteration in the amount or distribution of the mitochondrial network in myoblasts from the patients (Supplementary Fig. 4*A*). The levels of several integral components of the mitochondrial machinery, including the mitochondrial transcription factor A, TFAM, as well as different components of respiratory complexes I, II, III, and IV, and the subunit α of the ATP synthase, were also similar to those in control cells (Supplementary Fig. 4*B*). Moreover, using direct channeling of substrates to mitochondria in permeabilized cells, no differences could be seen between the patient fibroblasts or myoblasts and control subjects (Supplementary Fig. 5).

To determine whether the impairment in glucose- and pyruvate-driven mitochondrial respiration was specific to pyruvate channeling into mitochondria in a functional cellular context, we next examined oxygen consumption in intact myoblasts using malate as an alternative mitochondrial substrate. In this case, the TXNIP-deficient patient myoblasts showed comparable respiratory rates as control subjects, showing that malate can bypass the block of mitochondrial respiration using pyruvate (Fig. 3*E* and *F*). We also attempted to rescue respiration with methyl pyruvate, which has higher membrane permeability than pyruvate and enters directly into mitochondria, but also methyl pyruvate could not restore respiration in the patient cells, thereby indicating that there is a genuine block of respiration on pyruvate (Fig. 4). We also sent the patient-derived fibroblasts for analyses of pyruvate dehydrogenase activities, which were all found to be normal (patient 1: mean activity 0.6 nmol/mg protein/min; patient 2: mean activity 0.62 nmol/mg protein/min; and patient 3: mean activity 0.78 nmol/mg protein/min; normal reference values: 0.6–0.9 nmol/mg protein/min).

In order to validate that the observed phenotype of the patient-derived cells was indeed due to the lack of TXNIP expression, we next reconstituted patient-derived fibroblasts with functional TXNIP using stable retroviral transduction. This was done with fibroblasts rather than myoblasts as they are easier to culture and transduce. We first verified that TXNIP expression was established using the pBABE-TXNIP vector compared with non-transduced cells or negative control subjects using an empty pBABE vector (Fig. 5*A*). We next performed respiration analyses using these cells when cultured in regular medium, which revealed that the respiration in the patient-derived cells became indistinguishable from healthy control subjects upon reconstitution with TXNIP (Fig. 5*B* and *C*). The transduction did not affect

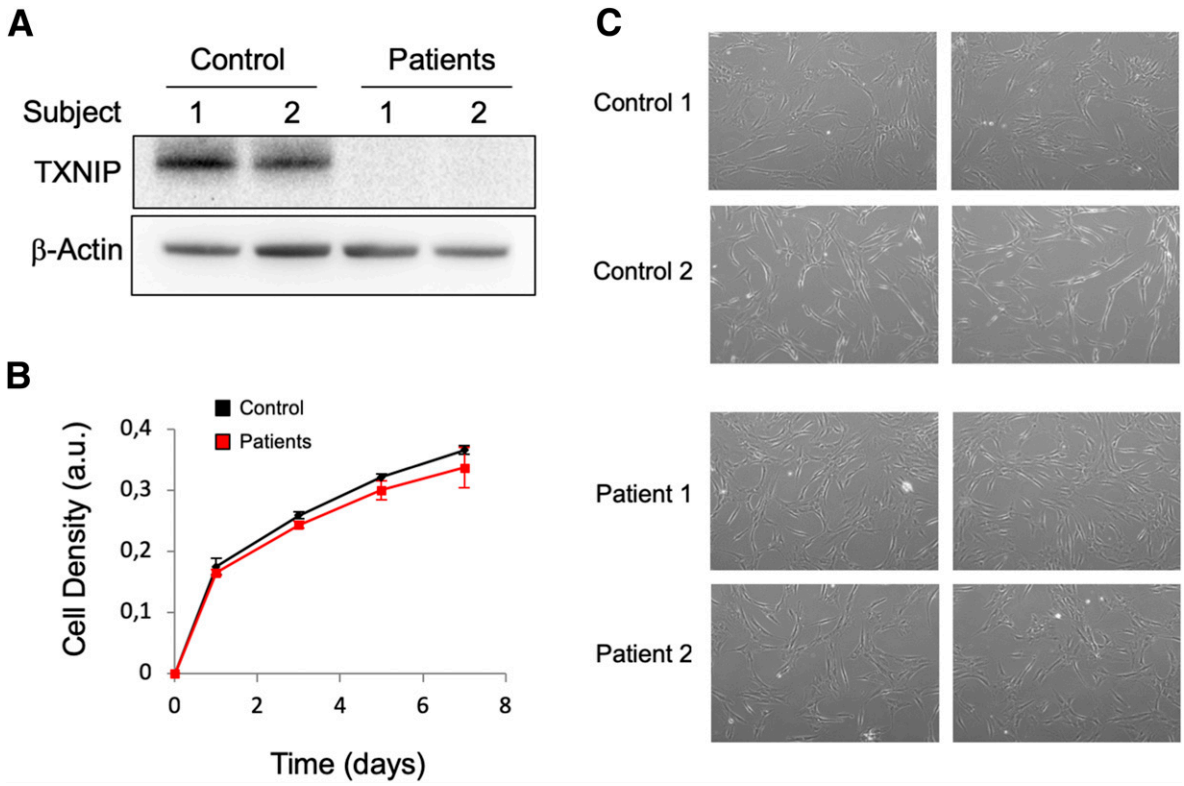

Figure 1—Primary myoblasts lacking TXNIP appear overtly normal. *A*: Western blot of TXNIP in primary myoblasts from two sets of primary myoblasts isolated from healthy subjects (Control 1 and 2) and primary myoblasts from patients with a point nonsense mutation in the *TXNIP* gene (Patients 1 and 2). β-Actin was used as loading control. Please note that this β-actin loading control is the same as depicted in Supplementary Fig. 4, since antibodies against TXNIP, TFAM, SDHA, and COX5a were probed in the same membrane. *B*: Growth of control (black) and *TXNIP*-null (red) primary myoblasts over 7 days. *C*: Bright-field images of primary myoblasts from patients and healthy donors. a.u., arbitrary units.

the capacity of the cells to respire on malate (Supplementary Fig. 6).

Collectively, these results strongly suggest that a lack of TXNIP does not lead to mitochondrial impairment per se, but rather to a specific deficiency in respiration on pyruvate.

DISCUSSION

In this study, we have presented the features of a natural human TXNIP deficiency with the cells from the affected individuals displaying transcriptional profiles suggestive of a strong basal activation of Nrf2 and diminished mitochondrial respiration on glucose and pyruvate. The results show that lack of TXNIP expression is nonlethal in humans and possibly that the metabolic consequences may be compatible with the notion that TXNIP is a promising antidiabetic drug target. It is important to note, however, that there is no indication suggesting that the patients described in this study have any other drivers promoting the development of diabetes (i.e., any theoretical inhibition of TXNIP in a patient with diabetes cannot be directly compared with the phenotype of the patients without diabetes lacking TXNIP described in this study). Notwithstanding this fact, we believe that some conclusions from our study deserve to be pointed out.

We could not find any evident increase in TXN activity in the patient-derived cells, which perhaps could have been hypothesized based upon the original TXNIP studies identifying the protein as an endogenous TXN inhibitor. TXNIP binding to TXN involves the formation of an intermolecular disulfide (37–39) that should be stable under our conditions of preparing cell lysates, thus suggesting that TXNIP was not severely impairing TXN activity in control cells under the conditions tested in this study or, conversely, that TXN activity is not necessarily increased upon loss of TXNIP. It should, however, be emphasized that several studies have suggested that the modulation of glucose homeostasis as regulated by TXNIP is not necessarily linked to its inhibition of TXN (40,41). Also, in cells from a *Txnip*-knockout mouse model, it was not possible to detect changes in Txn activities or protein levels (22), although overexpression of a *Txnip* variant binding Txn but not one incapable of binding Txn could restore a *Txnip*-null phenotype (20). It is not clear

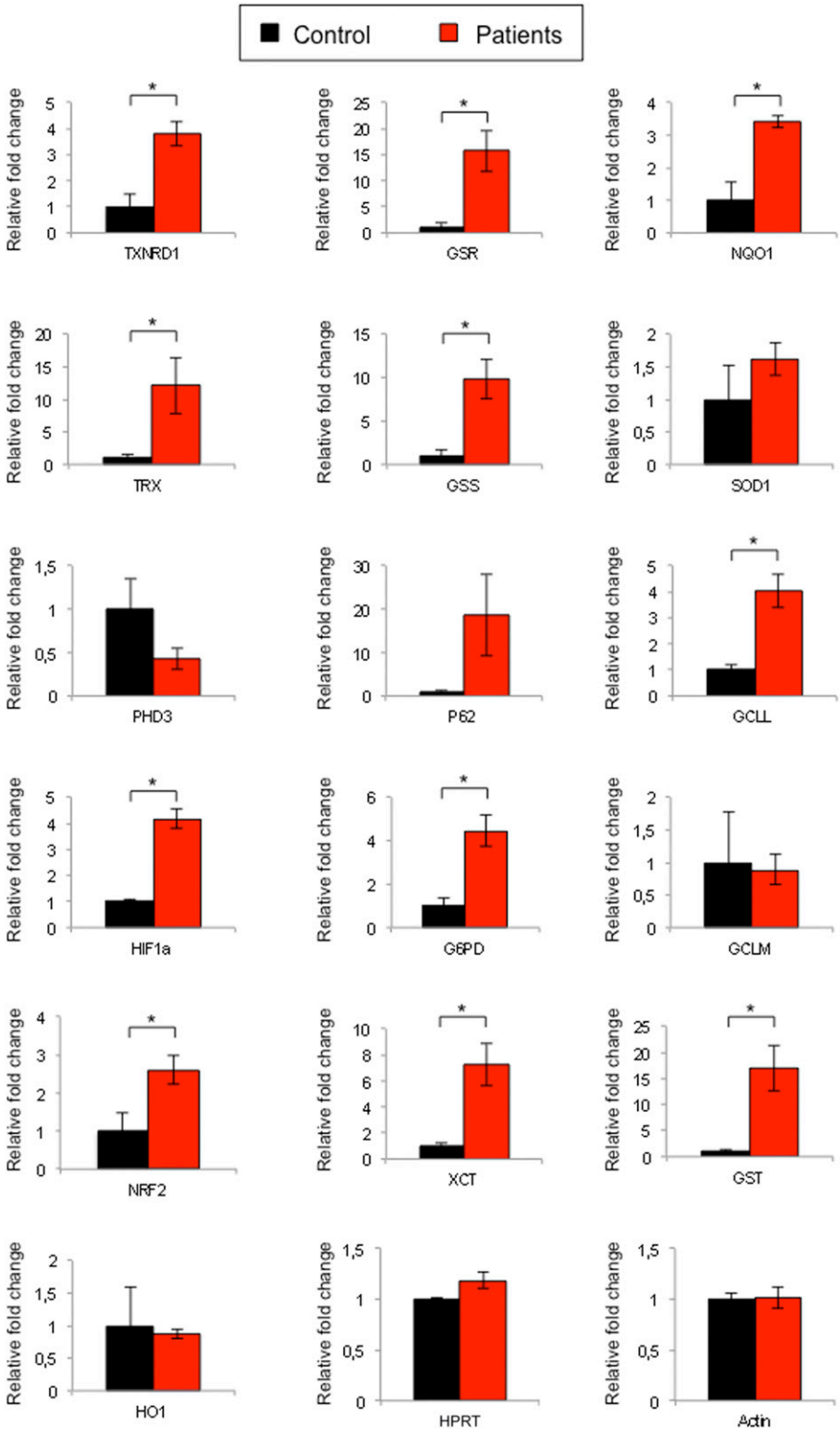

Figure 2—Strong basal activation of Nrf2 in TXNIP-null myoblasts. The graphs display the relative gene expression patterns for a selected set of mainly Nrf2 target genes as determined by quantitative RT-PCR in primary myoblasts from control subjects (black) and patients (red). Bars show mean ± SEM (n = 5 independent cultures of cells using two pooled cellular RNA samples each for either control subjects or patients; *$P < 0.05$). For information on full gene names and gene functions, please see www.genenames.org or www.genecards.org.

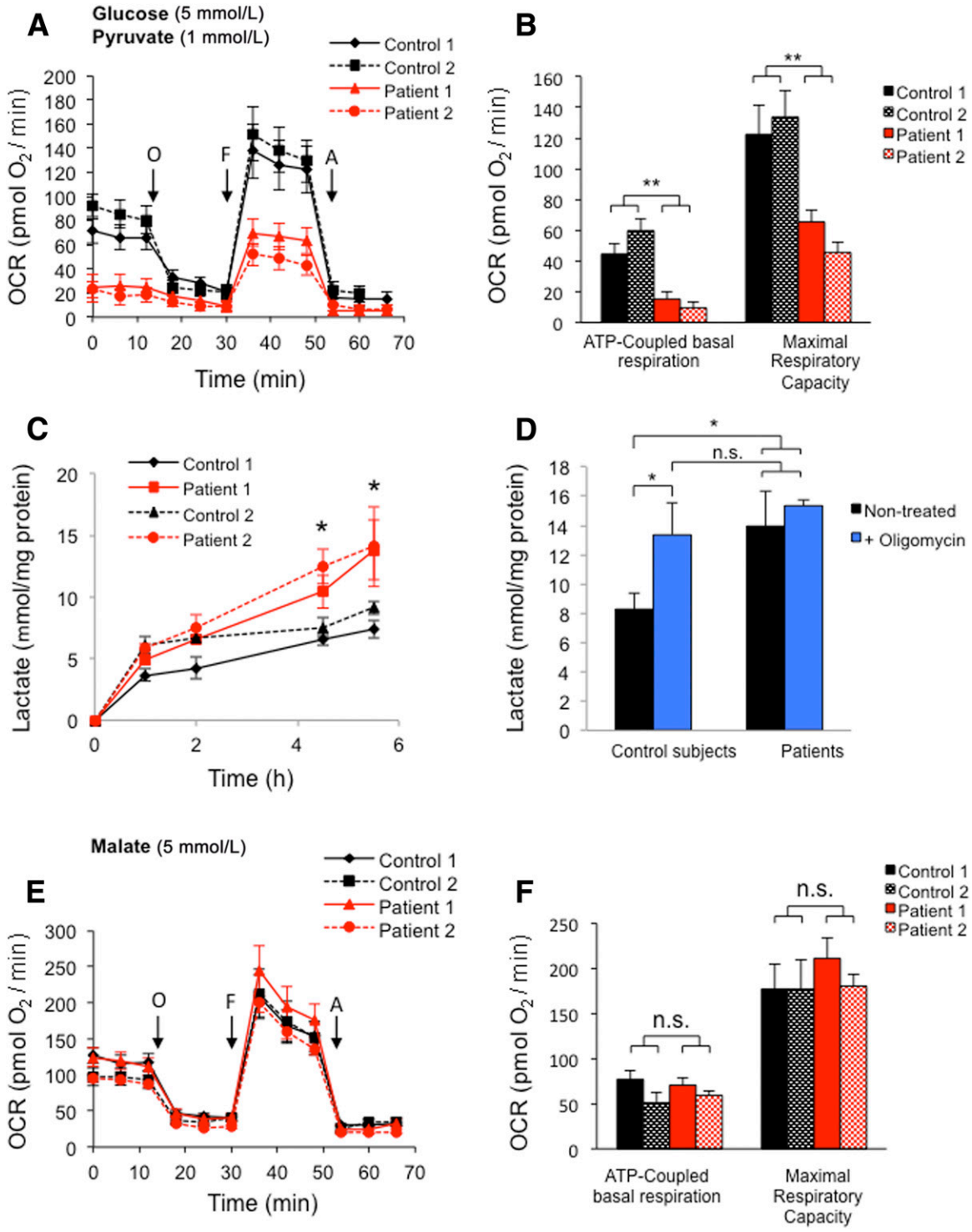

Figure 3—TXNIP-null myoblasts have deficient mitochondrial respiration on glucose and pyruvate but not on malate. *A*: Monitoring of OCR in real time in the presence of 5 mmol/L glucose and 1 mmol/L pyruvate using extracellular flux analysis in primary myoblasts from healthy donors (black) and patients (red). The sequential addition of oligomycin (O), FCCP (F), and antimycin (A) was used to determine ATP-coupled basal respiration and maximal respiratory capacity, respectively. *B*: Assessment of ATP-coupled basal respiration and maximal respiratory capacity in primary myoblasts from control subjects and patients, based on the results obtained in *A*. For *A* and *B*, data are represented as mean ± SEM (n = 4 independent experiments, 5–8 wells per genotype per experiment). *C*: Glycolysis-derived lactate production in primary myoblasts from control subjects (black) and patients (red). *D*: Lactate production at 6 h in primary myoblasts from control subjects and patients in the presence (blue) or absence (black) of the ATP synthase inhibitor oligomycin (5 μmol/L). For *C* and *D*, bars represent mean ± SEM (n = 3 independent experiments, 2 wells per set of cells per experiment). *E* and *F*: Monitoring of OCR, ATP-coupled basal respiration, and maximal respiratory capacity measured as in *A* and *B* but in the presence of 5 mmol/L malate instead of glucose and pyruvate. Data are represented as mean ± SEM (n = 3 independent experiments, 5–6 wells per set of cells per experiment) (*$P < 0.05$; **$P < 0.01$).

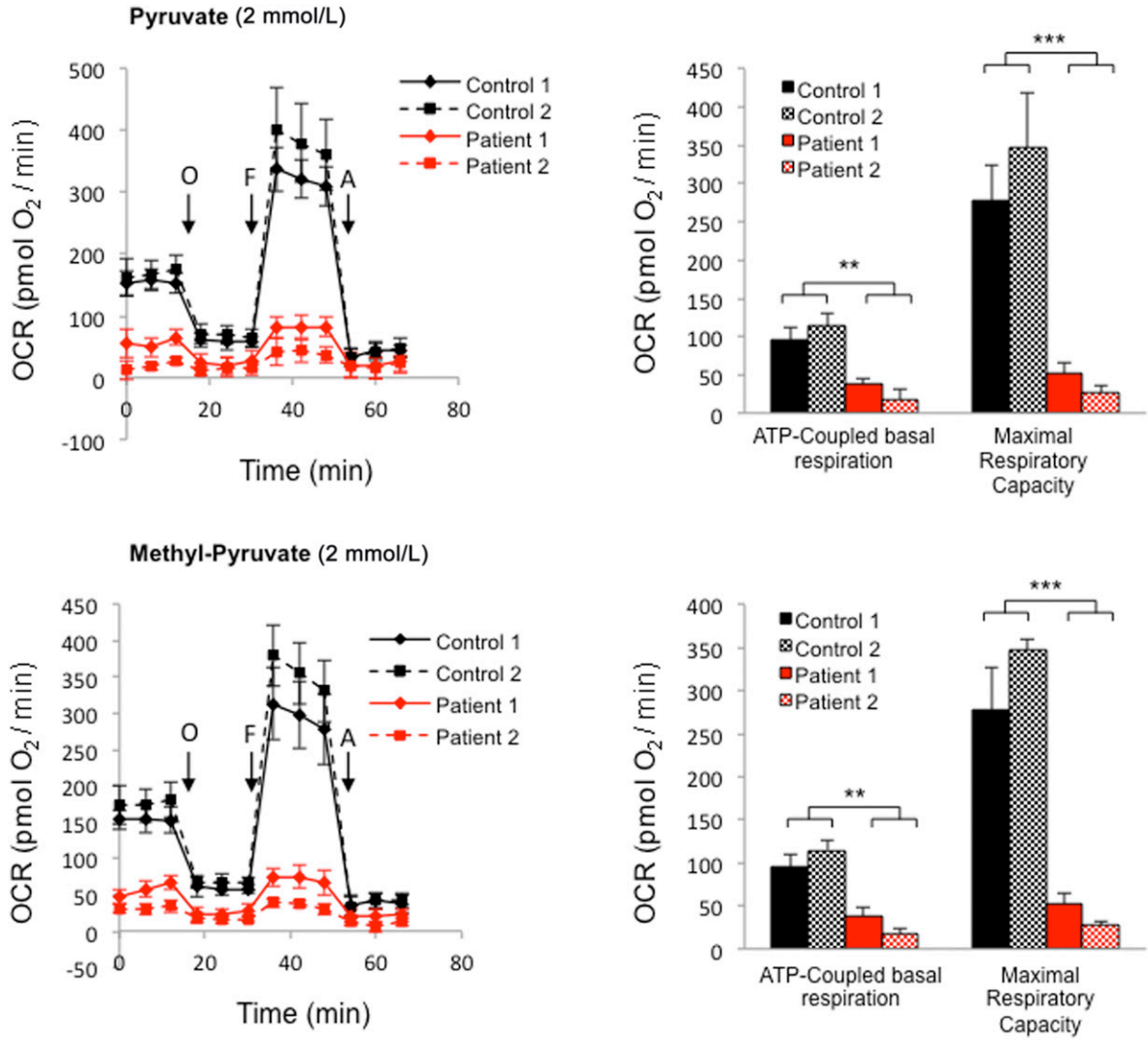

Figure 4— Lack of respiration in TXNIP-deficient myoblasts on pyruvate cannot be rescued by cell membrane–permeable methyl pyruvate. Monitoring of OCR in real time in the presence of 2 mmol/L pyruvate (top) or 2 mmol/L methyl pyruvate (bottom) using extracellular flux analysis in primary myoblasts from healthy donors (black) and patients (red). For details on the analyses, abbreviations, and statistics, see legend of Fig. 3*A*, *B*, *E*, and *F*. As is well illustrated in this figure, the deficiencies in respiration of patient-derived myoblasts (red) compared with control subjects (black) display very similar patterns irrespective of growth on pyruvate or on cell membrane permeable methyl pyruvate. $^{***}P < 0.005$.

whether that latter effect was truly due to Txn binding or to some other activity of Txnip that requires the same Cys residue to be intact. It should be noted that regulation of miRNA species or transcription factors are additional functions of TXNIP (42). Concerning transcription factor regulation, suppression of Nrf2 by TXNIP is perhaps important. TXNIP expression is directly repressed by Nrf2, and, conversely, TXNIP can possibly counteract Nrf2 activation (8,11). This activity of TXNIP is yet insufficiently characterized and requires further scrutiny, but is supported by our findings with a strong induction of many Nrf2 target genes in the TXNIP-deficient patient cells. It is interesting, however, that we could not detect altered TXN or TXNRD activities in the patient cells, since diminished TXNRD1 activity typically activates Nrf2 (12) but also that both TXN and TXNRD1 are Nrf2 target genes that would be expected to be upregulated upon Nrf2 activation. We indeed detected higher levels of TXN and TXNRD1 transcripts in the patient cells, but not higher protein or activity levels. Whether this particular expression profile is a unique consequence of TXNIP deletion is not known and should be studied further, as should the possible mechanisms leading to Nrf2 activation upon loss of TXNIP.

We found the inefficiency of the patient cells to use glucose and pyruvate for mitochondrial respiration, but accepting malate as an alternative substrate, to be a notable finding. This suggests that lack of TXNIP yields a rather specific deficiency in glucose utilization and not in mitochondrial function per se, at least in the cell types studied

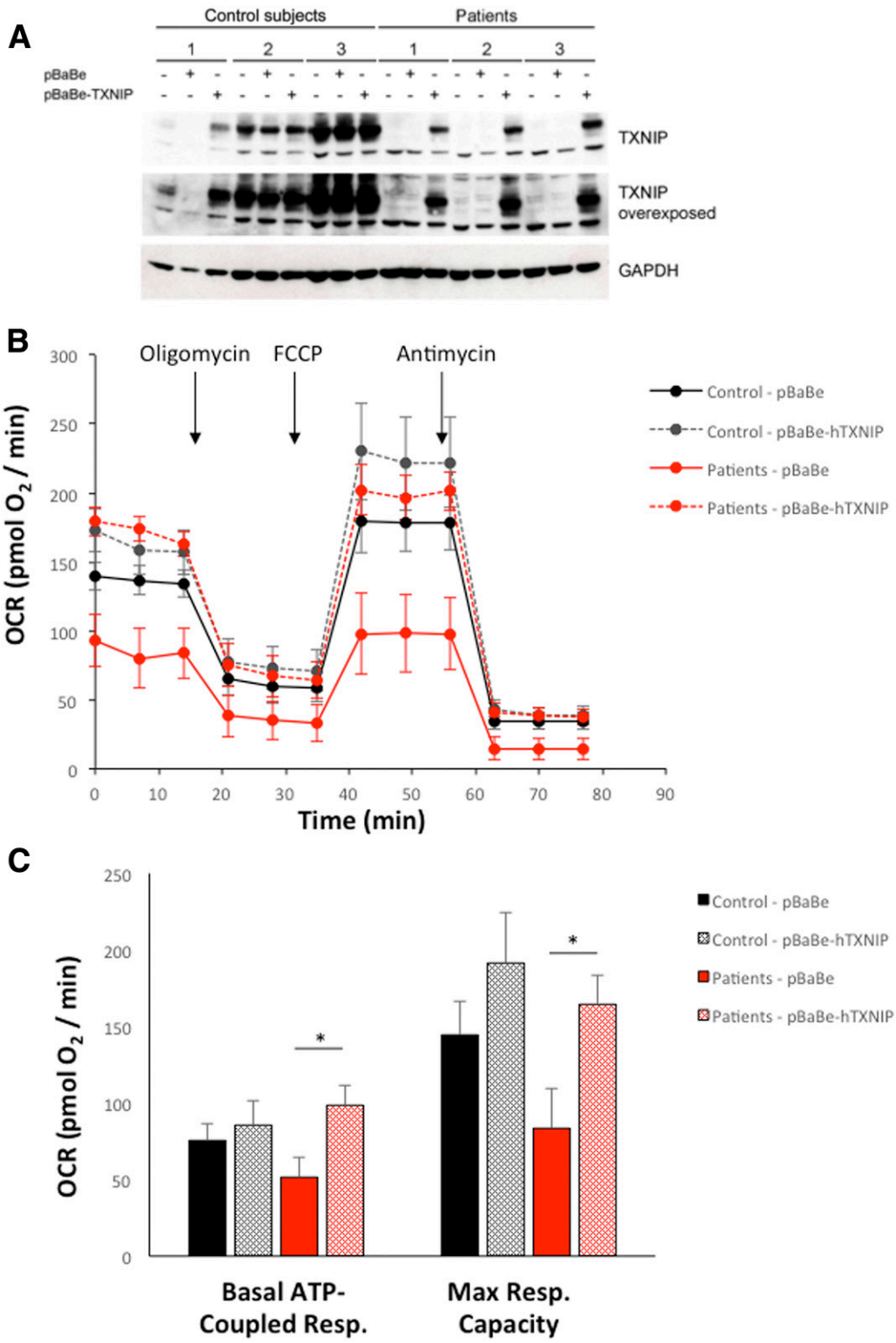

Figure 5— Reconstitution of TXNIP-null fibroblasts restores respiration on pyruvate. *A*: Immunoblot of TXNIP expression in control subject or patient cells either nontransduced or transduced with empty control vector pBaBe or with pBaBe-TXNIP–expressing vector, with detection of GAPDH used as loading control, as indicated in the figure. *B*: Monitoring of OCR in real time in the presence of 5 mmol/L glucose and 1 mmol/L pyruvate using extracellular flux analysis in primary myoblasts from healthy donors (black) and from patients (red), performed as in Fig. 3. In total, each cell line was analyzed in three independent plates performed on separate days with 5–6 wells per plate, thereby resulting in 15–18 recorded measurements per cell line. Data are represented as mean ± SEM ($n = 3$ independent experiments, 5–6 wells per cell type per experiment). *C*: Basal ATP-coupled respiration (Resp.) and maximal respiratory capacity derived from the experiment shown in *B*, defined as in Fig. 3 (*$P < 0.05$).

in this paper. The finding is partly consistent with studies in mice, showing that *Txnip* ablation leads to a deficiency in pyruvate dehydrogenase activity and a subsequent decrease in pyruvate-driven mitochondrial respiration, at least in cardiomyocytes (21). However, we could not find evidence of distorted pyruvate dehydrogenase activity in the patient-derived fibroblasts, and the mechanisms involved for the lack of pyruvate-driven respiration in these cells are thereby not fully explained. The metabolic shift perhaps relates to the findings in cancer cells, in which a constitutively upregulated Nrf2 yields a preference in glucose metabolism for anabolic pathways combined with glutamine catabolism, leading to increased production of lactate from malate through formation of pyruvate (43). This could yield a functional mitochondrial deficiency of malate, which was a reason for us to analyze mitochondrial respiration upon additional malate supplementation. It is thus possible that the increased lactic acidosis seen in the TXNIP-deficient patients is due to a combination of diminished usage of pyruvate by mitochondria, as well as increased production of pyruvate from malate derived from glutamine catabolism. In both cases, the increased levels of pyruvate would be expected to yield an increased production of lactate. It should be noted, however, that in this study, we have only been able to characterize primary myoblasts and fibroblasts from these patients, and it is possible that the metabolic pathways affected by a lack of TXNIP are different in other tissues, such as liver or pancreas. Indeed, both TXNIP and Nrf2 are known to display tissue-specific effects in their strong influences on metabolic pathways and tissue integrity (3,15,25,30). Total *Txnip* knockout in mice has, however, also been reported to yield increased serum lactate levels compared with control subjects, at least under fasting conditions (44).

The patients who we described in this study have undetectable levels of TXNIP protein, with lactic acidosis and low serum methionine as their common major presenting signs. Evidence of hypoglycemia, liver involvement, and muscle weakness were also noted but not in all three siblings. The lactic acidosis, with all three siblings responding well to the classical treatment with dichloroacetate, although this can have variable success in children (45), is likely to be explained by the inefficient respiration on pyruvate that we found using the patient-derived cells, but as of today, we have no explanation for the clinical presentation with low serum methionine. It should be noted that methionine can be an important source of reducing power through synthesis of glutathione, which is used in mice upon conditional deletion of *Txnrd1* in hepatocytes with or without concomitant deletion of *Txn* (46,47). Such increased usage of methionine should however not be needed in cells or tissues lacking TXNIP; on the contrary, the TXN system would be presumed to have increased activities if anything, thus minimizing the need for methionine as a source of reducing equivalents. However, because we also found Nrf2 to be activated in the patient-derived cells, it could be possible that an increased glutathione synthesis, as activated by Nrf2, would increase methionine usage. Other reasons for low serum methionine in the patients not related to cysteine or glutathione synthesis may involve some yet unidentified lack of a TXNIP-dependent process helping to maintain physiological serum methionine levels. In *Txnip*-null mice, the detrimental effects of methionine- and choline-deficient diet are aggravated compared with control subjects (48) but we are not aware of any study that has investigated functional links between TXNIP status and methionine levels in serum. This relationship is clearly another aspect of TXNIP deficiency that deserves to be further studied. It is perhaps likely that an altered metabolic flux of methionine in liver of the TXNIP-deficient patients is involved that, however, is difficult to experimentally probe in a clinical setting.

We conclude that the clinical and cellular phenotypes of patients lacking TXNIP suggest that this protein has rather specific regulatory effects in humans. Its deficiency is evidently nonlethal, and the major clinical presentations are lactic acidosis and low serum methionine, with little or no other overt pathophysiology. Glucose utilization for mitochondrial respiration in the patient-derived cells was impaired mainly due to a deficiency of the mitochondria to use pyruvate. These findings may thus collectively indicate that inhibition of TXNIP can indeed be beneficial in humans for the treatment of diabetes, as has been proposed, although it should be noted that a genetic lack of TXNIP in patients without diabetes does not necessarily mimic effects of drug-mediated TXNIP inhibition in therapy of diabetes. Possible main side effects of TXNIP inhibition in humans would, based upon our findings, be lactic acidosis and lowered serum methionine levels.

Funding. The authors received funding from Karolinska Institutet, The Swedish Research Council (2016-01082 to A.We., VR521-201-2571 and 2016-02179 to A.Wr., and 2013-765 and 2014-2603 to E.S.J.A.), the Swedish Cancer Society (2015/238 to E.S.J.A.), the Knut and Alice Wallenberg Foundation (KAW 2013.0026 and KAW 2014.0293 to A.We. and KAW 2015.0063 to E.S.J.A.), Stockholm County Council (20170022 to A.We.), the Spanish "Ministerio of Economía y Competitividad" (grant BFU2016-77634-R and "Ramón y Cajal" fellowship RYC-2014-15792), Diabetesfonden, and Alicia Koplowitz Foundation to A.G.-C. A.Wr. is a Ragnar Söderberg fellow in Medicine (M77/13).

Duality of Interest. No potential conflicts of interest relevant to this article were reported.

Author Contributions. Y.K.-J., C.V.-C., C.M., X.P., C.F., and A.G.-C. performed experiments and analyzed results. M.H., A.Wr., and A.We. had patient contacts and responsibilities for the clinical aspects of the study. A.We. and E.S.J.A. initiated and planned the study. C.F., A.Wr., A.G.-C., A.We., and E.S.J.A. jointly led the study. A.G.-C. and E.S.J.A. wrote the manuscript. Y.K.-J., C.V.-C., C.M., M.H., X.P., C.F., A.Wr., A.G.-C., A.We., and E.S.J.A. reviewed the manuscript and helped finalize the study. A.G.-C, A.We., and E.S.J.A. are the guarantors of this work and, as such, had full access to all of the data in the study and take responsibility for the integrity of the data and the accuracy of the data analysis.

References

1. Chen KS, DeLuca HF. Isolation and characterization of a novel cDNA from HL-60 cells treated with 1,25-dihydroxyvitamin D-3. Biochim Biophys Acta 1994; 1219:26–32
2. Nishiyama A, Matsui M, Iwata S, et al. Identification of thioredoxin-binding protein-2/vitamin D(3) up-regulated protein 1 as a negative regulator of thioredoxin function and expression. J Biol Chem 1999;274:21645–21650
3. Yoshihara E, Masaki S, Matsuo Y, Chen Z, Tian H, Yodoi J. Thioredoxin/Txnip: redoxisome, as a redox switch for the pathogenesis of diseases. Front Immunol 2014;4:514
4. Arnér ES. Focus on mammalian thioredoxin reductases–important selenoproteins with versatile functions. Biochim Biophys Acta 2009;1790:495–526
5. Tinkov AA, Bjørklund G, Skalny AV, et al. The role of the thioredoxin/thioredoxin reductase system in the metabolic syndrome: towards a possible prognostic marker? Cell Mol Life Sci 2018;75:1567–1586
6. Zhou J, Chng WJ. Roles of thioredoxin binding protein (TXNIP) in oxidative stress, apoptosis and cancer. Mitochondrion 2013;13:163–169
7. Abderrazak A, Syrovets T, Couchie D, et al. NLRP3 inflammasome: from a danger signal sensor to a regulatory node of oxidative stress and inflammatory diseases. Redox Biol 2015;4:296–307
8. Chong CR, Chan WP, Nguyen TH, et al. Thioredoxin-interacting protein: pathophysiology and emerging pharmacotherapeutics in cardiovascular disease and diabetes. Cardiovasc Drugs Ther 2014;28:347–360
9. Zhou R, Tardivel A, Thorens B, Choi I, Tschopp J. Thioredoxin-interacting protein links oxidative stress to inflammasome activation. Nat Immunol 2010;11: 136–140
10. Hou Y, Wang Y, He Q, et al. Nrf2 inhibits NLRP3 inflammasome activation through regulating Trx1/TXNIP complex in cerebral ischemia reperfusion injury. Behav Brain Res 2018;336:32–39
11. He X, Ma Q. Redox regulation by nuclear factor erythroid 2-related factor 2: gatekeeping for the basal and diabetes-induced expression of thioredoxin-interacting protein. Mol Pharmacol 2012;82:887–897
12. Cebula M, Schmidt EE, Arnér ES. TrxR1 as a potent regulator of the Nrf2-Keap1 response system. Antioxid Redox Signal 2015;23:823–853
13. Zhao C, Gillette DD, Li X, Zhang Z, Wen H. Nuclear factor E2-related factor-2 (Nrf2) is required for NLRP3 and AIM2 inflammasome activation. J Biol Chem 2014;289:17020–17029
14. Jiménez-Osorio AS, González-Reyes S, Pedraza-Chaverri J. Natural Nrf2 activators in diabetes. Clin Chim Acta 2015;448:182–192
15. Uruno A, Yagishita Y, Yamamoto M. The Keap1-Nrf2 system and diabetes mellitus. Arch Biochem Biophys 2015;566:76–84
16. Puca L, Brou C. A-arrestins - new players in Notch and GPCR signaling pathways in mammals. J Cell Sci 2014;127:1359–1367
17. Bodnar JS, Chatterjee A, Castellani LW, et al. Positional cloning of the combined hyperlipidemia gene Hyplip1. Nat Genet 2002;30:110–116
18. Donnelly KL, Margosian MR, Sheth SS, Lusis AJ, Parks EJ. Increased lipogenesis and fatty acid reesterification contribute to hepatic triacylglycerol stores in hyperlipidemic Txnip-/- mice. J Nutr 2004;134:1475–1480
19. Sheth SS, Castellani LW, Chari S, et al. Thioredoxin-interacting protein deficiency disrupts the fasting-feeding metabolic transition. J Lipid Res 2005;46: 123–134
20. Chutkow WA, Patwari P, Yoshioka J, Lee RT. Thioredoxin-interacting protein (Txnip) is a critical regulator of hepatic glucose production. J Biol Chem 2008;283: 2397–2406
21. Yoshioka J, Chutkow WA, Lee S, et al. Deletion of thioredoxin-interacting protein in mice impairs mitochondrial function but protects the myocardium from ischemia-reperfusion injury. J Clin Invest 2012;122:267–279
22. Yoshioka J, Imahashi K, Gabel SA, et al. Targeted deletion of thioredoxin-interacting protein regulates cardiac dysfunction in response to pressure overload. Circ Res 2007;101:1328–1338
23. Chutkow WA, Birkenfeld AL, Brown JD, et al. Deletion of the alpha-arrestin protein Txnip in mice promotes adiposity and adipogenesis while preserving insulin sensitivity. Diabetes 2010;59:1424–1434
24. Chen J, Hui ST, Couto FM, et al. Thioredoxin-interacting protein deficiency induces Akt/Bcl-xL signaling and pancreatic beta-cell mass and protects against diabetes. FASEB J 2008;22:3581–3594
25. Parikh H, Carlsson E, Chutkow WA, et al. TXNIP regulates peripheral glucose metabolism in humans. PLoS Med 2007;4:e158
26. Nagaraj K, Lapkina-Gendler L, Sarfstein R, et al. Identification of thioredoxin-interacting protein (TXNIP) as a downstream target for IGF1 action. Proc Natl Acad Sci U S A 2018;115:1045–1050
27. Soriano-Tárraga C, Jiménez-Conde J, Giralt-Steinhauer E, et al.; GENESTROKE Consortium. Epigenome-wide association study identifies TXNIP gene associated with type 2 diabetes mellitus and sustained hyperglycemia. Hum Mol Genet 2016;25:609–619
28. Florath I, Butterbach K, Heiss J, et al. Type 2 diabetes and leucocyte DNA methylation: an epigenome-wide association study in over 1,500 older adults. Diabetologia 2016;59:130–138
29. Kulkarni H, Kos MZ, Neary J, et al. Novel epigenetic determinants of type 2 diabetes in Mexican-American families. Hum Mol Genet 2015;24:5330–5344
30. Thielen L, Shalev A. Diabetes pathogenic mechanisms and potential new therapies based upon a novel target called TXNIP. Curr Opin Endocrinol Diabetes Obes 2018;25:75–80
31. Stranneheim H, Engvall M, Naess K, et al. Rapid pulsed whole genome sequencing for comprehensive acute diagnostics of inborn errors of metabolism. BMC Genomics 2014;15:1090
32. Wibom R, Hagenfeldt L, von Döbeln U. Measurement of ATP production and respiratory chain enzyme activities in mitochondria isolated from small muscle biopsy samples. Anal Biochem 2002;311:139–151
33. Salcedo M, Cuevas C, Alonso JL, et al. The marine sphingolipid-derived compound ES 285 triggers an atypical cell death pathway. Apoptosis 2007;12:395–409
34. Peng X, Mandal PK, Kaminskyy VO, Lindqvist A, Conrad M, Arnér ES. Sec-containing TrxR1 is essential for self-sufficiency of cells by control of glucose-derived H2O2. Cell Death Dis 2014;5:e1235
35. Giménez-Cassina A, Garcia-Haro L, Choi CS, et al. Regulation of hepatic energy metabolism and gluconeogenesis by BAD. Cell Metab 2014;19:272–284
36. Peng X, Giménez-Cassina A, Petrus P, Conrad M, Rydén M, Arnér ES. Thioredoxin reductase 1 suppresses adipocyte differentiation and insulin responsiveness. Sci Rep 2016;6:28080
37. Hwang J, Suh HW, Jeon YH, et al. The structural basis for the negative regulation of thioredoxin by thioredoxin-interacting protein. Nat Commun 2014; 5:2958
38. Fould B, Lamamy V, Guenin SP, et al. Mutagenic analysis in a pure molecular system shows that thioredoxin-interacting protein residue Cys247 is necessary and sufficient for a mixed disulfide formation with thioredoxin. Protein Sci 2012; 21:1323–1333
39. Patwari P, Higgins LJ, Chutkow WA, Yoshioka J, Lee RT. The interaction of thioredoxin with Txnip. Evidence for formation of a mixed disulfide by disulfide exchange. J Biol Chem 2006;281:21884–21891
40. Spindel ON, World C, Berk BC. Thioredoxin interacting protein: redox dependent and independent regulatory mechanisms. Antioxid Redox Signal 2012;16:587–596
41. Patwari P, Chutkow WA, Cummings K, et al. Thioredoxin-independent regulation of metabolism by the alpha-arrestin proteins. J Biol Chem 2009;284: 24996–25003
42. Jing G, Westwell-Roper C, Chen J, Xu G, Verchere CB, Shalev A. Thioredoxin-interacting protein promotes islet amyloid polypeptide expression through miR-124a and FoxA2. J Biol Chem 2014;289:11807–11815
43. Mitsuishi Y, Taguchi K, Kawatani Y, et al. Nrf2 redirects glucose and glutamine into anabolic pathways in metabolic reprogramming. Cancer Cell 2012;22:66–79
44. Hui ST, Andres AM, Miller AK, et al. Txnip balances metabolic and growth signaling via PTEN disulfide reduction. Proc Natl Acad Sci U S A 2008;105:3921–3926

45. Mangal N, James MO, Stacpoole PW, Schmidt S. Model informed dose optimization of dichloroacetate for the treatment of congenital lactic acidosis in children. J Clin Pharmacol 2018;58:212–220
46. Prigge JR, Coppo L, Martin SS, et al. Hepatocyte hyperproliferation upon liver-specific co-disruption of thioredoxin-1, thioredoxin reductase-1, and glutathione reductase. Cell Reports 2017;19:2771–2781
47. Eriksson S, Prigge JR, Talago EA, Arnér ES, Schmidt EE. Dietary methionine can sustain cytosolic redox homeostasis in the mouse liver. Nat Commun 2015; 6:6479
48. Ahsan MK, Okuyama H, Hoshino Y, et al. Thioredoxin-binding protein-2 deficiency enhances methionine-choline deficient diet-induced hepatic steatosis but inhibits steatohepatitis in mice. Antioxid Redox Signal 2009;11:2573–2584